ACS APPLIED MATERIALS & INTERFACES

Research Article

www.acsami.org

Five Orders of Magnitude Reduction in Energy Coupling across Corrugated Graphene/Substrate Interfaces

Xiaoduan Tang, Shen Xu, Jingchao Zhang, and Xinwei Wang*

Department of Mechanical Engineering, Iowa State University, 2010 Black Engineering Building, Ames, Iowa 50011, United States

ABSTRACT: A normal full-contact graphene/substrate interface has been reported to have a thermal conductance in the order of 10^8 $Wm^{-2}K^{-1}$. The reported work used a sandwiched structure to probe the interface energy coupling, and the phonon behavior in graphene was significantly altered in an undesirable way. Here, we report an intriguing study of energy coupling across unconstrained graphene/substrate interfaces. Using novel Raman-based dual thermal probing, we directly measured the temperature drop across the few nm gap interface that is subjected to a local heat flow induced by a second laser beam heating. The thermal conductance (G_t) for graphene/Si and graphene/SiO_2 interfaces is determined as 183 ± 10 and 266 ± 10 $Wm^{-2}K^{-1}$. At the graphene/Si interface, G_t is 5 orders of magnitude smaller than that of full interface contact. It reveals the remarkable effect of graphene corrugation on interface energy coupling. The measurement result is elucidated by atomistic modeling of local corrugation and energy exchange. By decoupling of graphene's thermal and mechanical behavior, we obtained the stress-induced Raman shift of graphene at around 0.1 cm^{-1} or less, suggesting extremely loose interface mechanical coupling. The interface gap variation is evaluated quantitatively on the basis of corrugation-induced Raman enhancement. The interface gap could change as much as 1.8 nm when the local thermal equilibrium is destroyed.

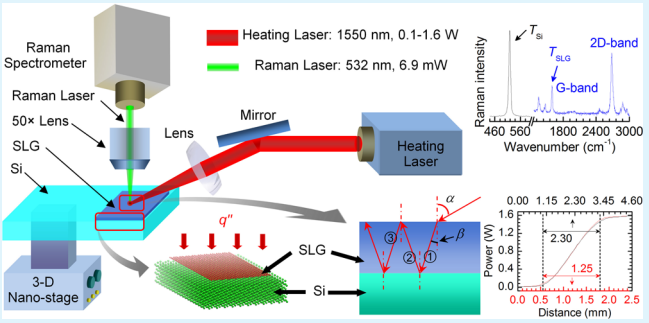

KEYWORDS: *unconstrained graphene interface, energy coupling, thermal conductance, nanoscale thermal probing, corrugation*

1. INTRODUCTION

As a two-dimensional material, graphene exhibits unique physical properties, which give the opportunity for broad potential applications.[1−4] Measurements of thermal conductivity of graphene revealed a high value from 630 to 5300 $Wm^{-1}K^{-1}$ in a temperature range of 300−600 K.[5−8] Molecular dynamics (MD) simulations determined an even higher thermal conductivity from 8,000 to 10,000 $Wm^{-1}K^{-1}$ at room temperature for graphene sheets.[9] Balandin reviewed the thermal properties of graphene and indicated the prospects of applications of graphene for thermal design of electronics.[10] The ultrahigh thermal conductivity of graphene prompts potential applications for heat removal in semiconductor devices.[5,11−13] It is possible for this two-dimensional material to effectively dissipate heat in the next generation 3-D electronics. In its application, graphene is either supported by a bulk substrate or embedded in a 3-D structure, for a two-dimensional material cannot exist in the free-standing state. Heat dissipation in the in-plane direction would be greatly impeded due to the thin thickness of graphene (0.35 nm for a single layer).[5,6] The thermal transport via the interface to the adjacent materials plays a major role in heat dissipation for graphene-based electronics. Therefore, the knowledge of energy coupling at the interface is important to evaluate this out-of-plane heat dissipation.

To this end, very little research has been done on thermal transport at the interface between graphene and its substrate.[14−18] The first work by Chen et al. used a second metal coating (Au) on a sandwiched graphene between two SiO_2 layers to facilitate the measurement with the 3ω technique.[14] Koh et al. and Hopkins et al. reported the thermal conductance at Au/Ti/graphene/SiO_2 and Al/graphene/SiO_2 interfaces.[15,16] In these studies, the graphene was sandwiched between structures, and the flexural phonon behavior was strongly constrained. Also, the graphene/substrate contact can be significantly altered during this sandwiched structure preparation. Mak et al. in 2010 determined that the thermal conductance of the graphene/SiO_2 interface ranged from 2,000 to 11,000 $Wcm^{-2}K^{-1}$.[17] The large dispersion reflected the relatively poorly defined nature of interface between exfoliated graphene and SiO_2. Work by Yue et al. reported an anomalous interfacial thermal resistance as 5.30×10^{-5} K m^2 W^{-1} between epitaxial graphene and SiC.[18] The reason was speculated to be the delamination of graphene and SiC at the interface under heating. The contact condition at the graphene/substrate interface is a main factor in determining the interfacial phonon coupling and energy exchange. Molecular dynamics simulations have been carried out to provide a fundamental understanding on heat transfer across interfaces between graphene sheets and SiC substrates.[18−20] In the study of free-standing graphene, it has been demonstrated that ripples are

Received: November 26, 2013
Accepted: January 29, 2014
Published: January 29, 2014

   dx.doi.org/10.1021/am405388a | *ACS Appl. Mater. Interfaces* 2014, 6, 2809−2818

an intrinsic feature of graphene sheets.[21] Intrinsic and extrinsic corrugation of graphene on SiO_2 was later examined and confirmed.[22] It was found that graphene is only partly bonded with its substrate and to some extent freely suspended on the substrate. Further research is necessary to simultaneously explore the interfacial contact and energy coupling between graphene and its substrate, and such research has been very rare to date.

In this work, the interface between graphene and its substrate is probed at the atomic level using Raman spectroscopy with the presence of an energy flow from graphene to the substrate. The thermal conductance of the interface between chemical vapor deposition (CVD) graphene and Si/glass is evaluated and complemented by atomistic scale modeling. The nanoscale rough contact between graphene and substrate is uncovered for the first time from four aspects: the anomalously weak interfacial energy coupling, localized stress analysis/mechanical coupling, optical interference at the interface under the effect of localized heating, and atomic force microscopy (AFM) imaging of surface morphology.

2. EXPERIMENTAL DETAILS

Figure 1 shows a schematic of the experimental setup for interfacial energy coupling characterization between graphene and Si substrate. The substrate is Si, which the heating laser (1550 nm) cannot go through from its rough back surface. The Si substrate used in this experiment has no thermal oxide SiO_2 layer on top. For a transparent glass substrate, a slightly different experiment is designed and will be detailed later. A single layer CVD graphene (SLG) on silicon sample (ACS Material) is placed on a 3-D nanostage (MAX311D, Thorlabs). The piezoelectric actuator of the nanostage is controlled in a feedback mode. The stability is significantly improved, and the positioning resolution is down to 5 nm. The high resolution and stability of the stage reduces the possible noise in the Raman spectra to a great degree, which is critical to the success of our measurements. A probing laser (λ = 532 nm) from a confocal Raman system irradiates the sample from the top. The Raman spectrometer (Voyage, B&W Tek) is confocal with a microscope (Olympus BX51). The spot size of the Raman laser focused through a 50× objective lens is $2 \times 4\ \mu m^2$, which is determined by using a blade method. The Raman laser power is so low (6.9 mW) that the temperature rise induced by the Raman laser is negligible. Mainly, the sample is heated up by a second (heating) laser (λ = 1550 nm) with a continuous energy power tunable up to 2 W. The laser propagation direction is 60° to the vertical direction (α = 60° as shown in Figure 1) from above the sample, while the graphene is in the horizontal plane.

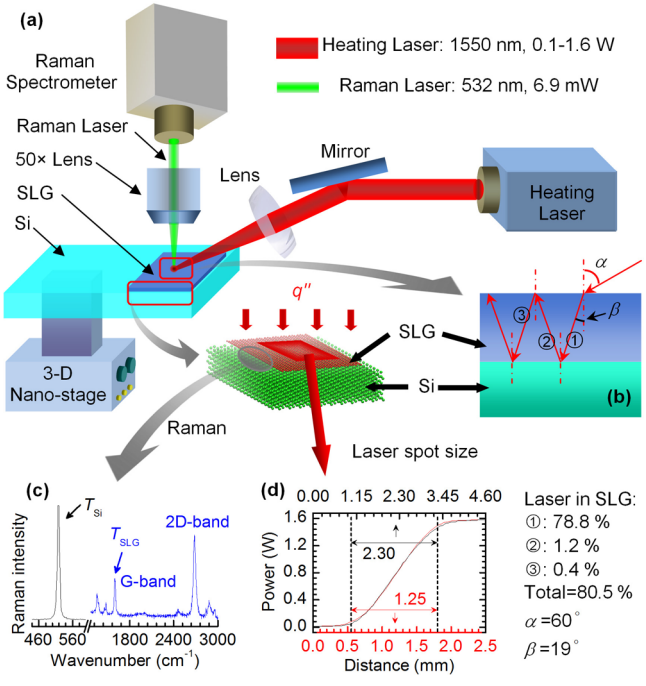

Figure 1. Schematic of the experimental setup for characterizing of the SLG/Si interface energy coupling. (a) A SLG/Si sample is heated up by a laser (λ = 1550 nm) from above with an incident angle of 60°. Raman signals of SLG and Si are excited by a Raman laser and collected with a Raman spectrometer. The position of the sample is controlled by a 3-D nanostage with a resolution of 5 nm. The graphene layer absorbs laser energy and dissipates heat to the Si substrate through their interface. (b) The heating laser propagation path and the accumulated energy passing through the graphene. (c) Temperatures of both SLG and Si can be determined simultaneously by a Raman spectrum. (d) The spot size of the heating laser on the sample is $2.30 \times 1.25\ mm^2$ with power varying from 0.1 to 1.6 W.

The heating laser is focused by an optical lens before it reaches the sample, and the final focal spot size is $2.30 \times 1.25\ mm^2$ (shown in Figure 1d). Within the spot size, 90% of the laser energy is covered. The light absorption in graphene can be calculated from Dirac fermions. For a single layer, 2.3% of laser light is absorbed.[23] After reaching the surface of the graphene, the laser light is refracted and reflected multiple times at the air/SLG and SLG/Si interfaces. The refractive indices of SLG and Si are 2.69 and 3.47, respectively. About 1.85% of the laser energy is absorbed in the graphene layer. The detailed path and absorbing percentage of the laser light is depicted in Figure 1b. Little laser energy is absorbed in the silicon substrate. At λ = 1550 nm, the heating photon energy is less than the bandgap of silicon, so the absorption in silicon is very small. The graphene layer is heated up by the heating laser and dissipates heat in three directions: one part crosses the plane to the interface, the second part dissipates along the graphene layer in the lateral direction, and the third part dissipates to the adjacent air via convection and radiation. In our experiment, the laser heating area is very large (1−2 mm) and the thermal probing area is very small (2−4 μm) and is in the middle of the heating region. Little temperature gradient and heat transfer exists in the in-plane direction in this μm central region. Also, the heat transfer to the adjacent air via radiation and convection is negligible in comparison with that across the graphene/Si interface. Heat is dissipated across the interface to the substrate. The temperature of the substrate would then increase. As the graphene layer is bonded with the substrate via van der Waals force (vdW), which is a loose contact, there would be large thermal contact resistance (small thermal conductance) between them. To determine the thermal conductance across this weak contact, Raman spectra of graphene and silicon substrate are obtained during laser heating. The graphene is confirmed to be a single layer according to the Raman intensity ratio of 2D peak and G peak shown in Figure 1c.[24] The Raman integration times for the silicon and graphene are 2 and 40 s, respectively. On the basis of the Raman signals of graphene and silicon, the temperatures of both layers are determined under different laser energies.

The Rama spectra are affected by factors including power of heating laser, focal level of Raman laser, stability of sample, and other equipment factors. In the measurement, the focal level of the Raman laser is first determined. When the Raman laser is focused on the graphene layer, the intensity of G peak is strong. A group of Raman spectra are obtained at several focal levels in the vertical direction. The background signal is subtracted to achieve sound Raman spectrum. The sample is fixed at the focal level that gives the highest graphene G peak intensity. During Raman spectrum acquisition, only the power of the heating laser is increased. No equipment is touched or changed. The effects of environmental changes are eliminated. It ensures the maximum measurement accuracy. In the measurement, the Raman laser also heats up the graphene and substrate. The heating induced by the Raman laser does not affect the results, however. First, all the results are obtained without changing the power of the Raman laser. The temperature change observed versus the heating laser power is only induced by the heating laser while the effect of Raman laser is subtracted in the linear fitting process (detailed later). Second, the power of the Raman laser (6.9 mW) is much smaller than that of the heating laser

dx.doi.org/10.1021/am405388a | ACS Appl. Mater. Interfaces 2014, 6, 2809−2818

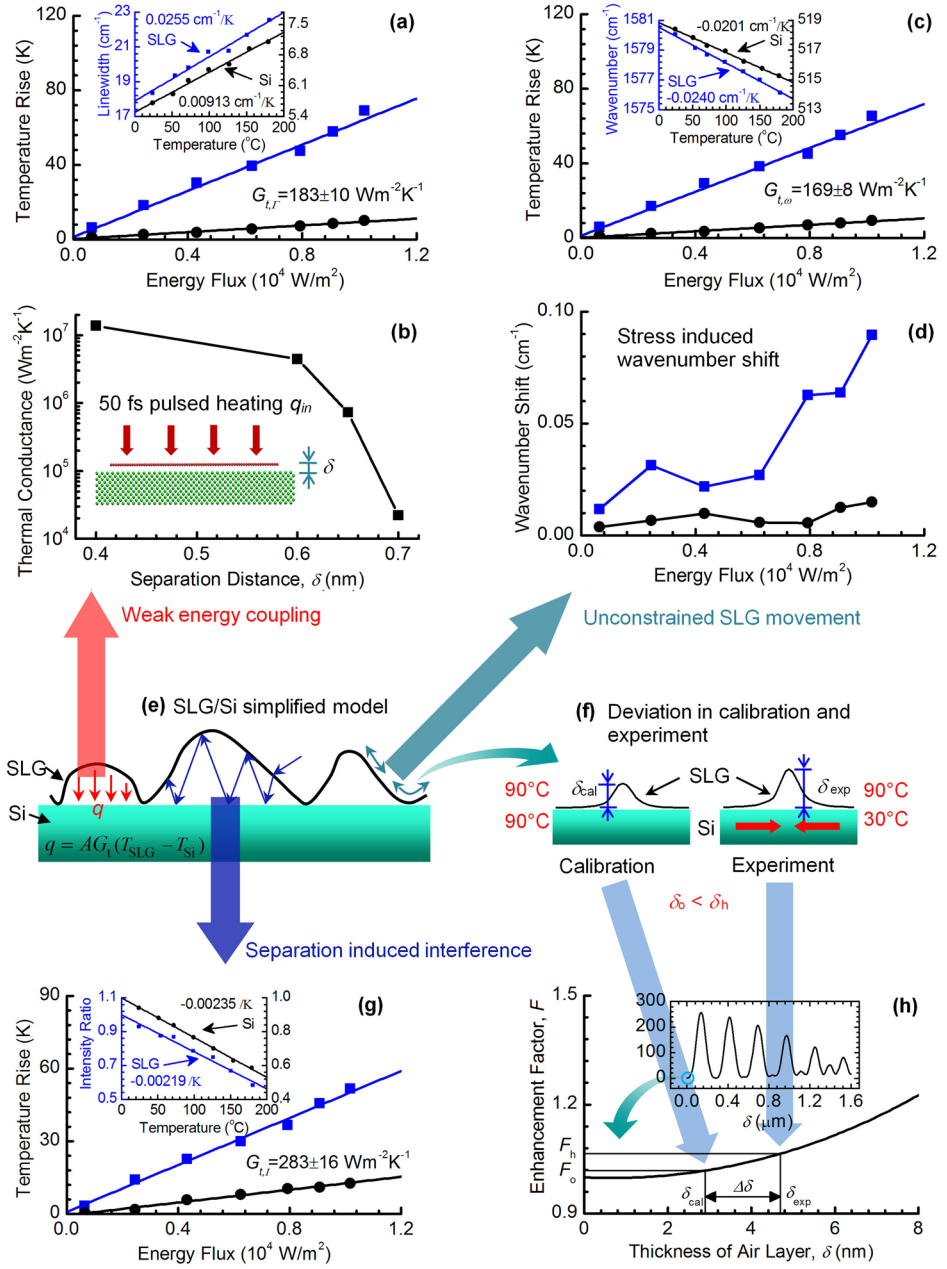

Figure 2. Nanoscale rough contact at the SLG/Si interface. (a) Thermal conductance (energy coupling rate) at the SLG/Si interface determined by linewidth broadening. The inset shows the calibration results of the temperature dependence of linewidth for G-band of SLG and Si. (b) Interfacial thermal conductance/energy coupling weakening effect by separation widening between SLG and Si. Atomic configuration of the system is shown in the inset. The thermal conductance decreases rapidly with increasing δ and reaches a level of 10^4 $Wm^{-2}K^{-1}$ when δ = 0.7 nm. (c) The linear fitting for temperature rise of SLG and Si against heating laser heat flux based on wavenumber softening. The inset shows the calibration results for wavenumber softening against temperature. (d) Stress induced wavenumber shift for SLG and Si. Very little stress is experienced by SLG and Si. (e) A simplified schematic of the SLG/Si interface for study of weak energy coupling, unconstrained SLG movement, and separation induced interference at the interface. (f) Deviation of the thickness of the separation layer in the experiment and calibration due to the thermal expansion mismatch between SLG and Si. (g) The temperature rise of SLG and Si against heating laser heat flux based on intensity decrease. The inset shows the calibration results. (h) Increment of the Raman intensity enhancement factor (F) of SLG with the thickness of separation layer (δ). δ is estimated to increase from 2.9 to 4.7 nm during the laser heating experiment. The inset shows the variation of F for a large range of δ. blue ■: SLG; black ●: Si.

(0.1−1.6 W). Thus, the temperature rise induced by the Raman laser is negligible.

3. RESULTS AND DISCUSSION

3.1. Weak Interfacial Energy Coupling between Graphene and Si. *3.1.1. Interface Thermal Conductance Characterization.* First of all, we present and discuss the characterization of energy coupling between graphene and Si. A single layer graphene on silicon substrate (ACS Material) is used in the experiments. The graphene is fabricated on copper first by using the CVD method and transferred to a silicon substrate. Raman intensity, wavenumber, and linewidth all can be employed to probe the temperature of materials. For graphene and silicon, the Raman intensity and wavenumber decrease, and linewidth broadens as their temperatures rise. Since linewidth is of close relevance with phonon lifetime, it is strongly affected by

dx.doi.org/10.1021/am405388a | ACS Appl. Mater. Interfaces 2014, 6, 2809−2818

temperature with negligible effect from stress. Therefore, the linewidth method can be used to determine the temperature of both materials and then to evaluate the interface thermal conductance. For wavenumber, previous research indicates that it is also dependent on the local stress in materials. Therefore, the temperature based on wavenumber is different from that based on linewidth if a local stress exists. For Raman intensity, the light interference at the graphene/substrate interface (if local spacing exists) is an influencing factor in addition to temperature. Interference at the interface enhances the Raman intensity.

The temperature coefficients of graphene and silicon against Raman linewidth were calibrated first in order to determine the local temperature during experiment, as shown in the inset of Figure 2a. Details of the calibration are given in 5.1 Thermal Probing and Raman Calibration. The thermal conductance at the SLG/Si interface is determined as $G_t = q''/(T_{SLG} - T_{Si})$, where T_{SLG} and T_{Si} are temperatures of SLG and Si and q'' is the heat flux. Since the determination of G_t from a single point is subject to more uncertainties, seven laser energy fluxes are used in the experiments to improve the accuracy. The temperature rise in Figure 2a is the value relative to room temperature. The effect of the Raman laser heating is subtracted since the Raman spectrum with Raman laser heating is used as the base to evaluate the linewidth change when the heating laser is applied. The temperature rise has a positive linear relationship with the energy flux. The fitted slopes for SLG and Si are 6.41×10^{-3} and 9.50×10^{-4} Km^2W^{-1}, respectively. Then, the interfacial thermal conductance is calculated as $G_t = 1/(T'_{SLG} - T'_{Si})$, where T'_{SLG} and T'_{Si} are fitting slopes of temperature against heat flux for SLG and Si, respectively. For the SLG/Si interface, the thermal conductance is determined as 183 $Wm^{-2}K^{-1}$, a very low value indicating very poor local energy coupling. For radiation from the graphene surface, the effective heat transfer coefficient is $h_r = 4\varepsilon\sigma T^3 = 0.14$ $Wm^{-2}K^{-1}$, where $\varepsilon = 0.023$ is emissivity of SLG,[23] $\sigma = 5.67 \times 10^{-8}$ $Wm^{-2}K^{-4}$, and $T = 300$ K. Thus, the measured thermal conductance is orders of magnitude larger than the one by the radiation between graphene and Si, and it is largely due to the interfacial energy coupling by atomic bonds. The equivalent interface thermal resistance is 5.46×10^{-3} Km^2W^{-1}. The resistance is five orders larger than the theoretical value of 3.52×10^{-8} Km^2W^{-1} at perfect contact between SLG and Si.[25] It indicates that the equivalent area of perfect contact between SLG and Si only consists of 6.5×10^{-6} of the whole contact area. The local energy coupling is extremely different from that at perfect contact conditions. The uncertainty of thermal conductance is analyzed according to the standard error of the linear fitting, and the value is 9.7 $Wm^{-2}K^{-1}$.

As shown in Figure 2a, the temperature rise of Si is relatively high while our theoretical analysis shows it should have a very low temperature rise due to its high thermal conductivity. This is because the back side of Si is unpolished. Some of the laser energy is absorbed at the rough surface of Si. In the measurement, the temperature of Si is an average temperature within the focal depth of the Raman probing laser. It is not the temperature immediately next to the Si surface. The skin depth of the Raman laser in silicon is $\tau = \lambda/(4\pi\kappa)$, where λ is the wavelength of the laser and κ is the extinction coefficient. At $\lambda = 532$ nm, $\kappa = 0.0516$ for silicon, and $\tau = 820$ nm. The thermal conductivity of Si is $k = 148$ $Wm^{-1}K^{-1}$. As the Raman excitation laser is focused on the Si surface, the measured temperature of Si can be estimated as $T_{exp} = \int_0^\infty T e^{(-x/(\tau/2))} dx / \int_0^\infty e^{(-x/(\tau/2))} dx = T|_{x=\tau/2}$, where x is the distance from Si surface and τ is the skin depth. This means the temperature of Si measured in the experiment is equal to the value at $x = \tau/2 = 410$ nm, a distance very close to the Si surface. The heat conduction resistance of Si across this distance is 5.54×10^{-9} Km^2W^{-1}. This value is significantly smaller than the measured interfacial thermal resistance of 5.46×10^{-3} Km^2W^{-1}. In conclusion, the little thermal resistance of the Si region has negligible effect on the total interfacial thermal conductance measurement.

3.1.2. Result Interpretation Based on Atomistic Modeling of Interface Energy Coupling. The measured thermal conductance at the SLG/Si interface is very small. For a normal full-contact interface with vdW force bond, a thermal conductance in the order of 10^8 $Wm^{-2}K^{-1}$ is expected. Our measured thermal conductance indicates very poor localized energy coupling. We speculate that a lot of areas at the graphene/Si interface have very poor contact, like some separations as delineated in Figure 2e. To further elucidate the interfacial thermal conductance change against the SLG/Si separation, molecular dynamics simulation is carried out by using the large-scale atomic/molecular massively parallel simulator (LAMMPS) package.[26] A silicon layer with dimensions of $5.8 \times 20.0 \times 5.4$ nm^3 is built, and the supported graphene nanoribbon (GNR) is 4.1×18.3 nm^2. Four cases with separation distances (δ) of 0.4, 0.6, 0.65, and 0.7 nm are calculated, and the thermal conductance results are shown in Figure 2b. Details of the simulation are provided in 5.2 Result Interpretation Based on Atomistic Modeling of Interface Energy Coupling. When the separation distance between graphene and Si substrate increases, the interatomic forces between these two materials decrease quickly. As a result, the thermal energy coupling between graphene and the Si system becomes so low, eventually leading to a much smaller thermal conductance. For δ equal to 0.6, 0.65, and 0.7 nm, the interfacial thermal conductance is 4.44×10^6, 7.30×10^5, and 2.21×10^4 $Wm^{-2}K^{-1}$, respectively. Such results strongly demonstrate that the interfacial thermal conductance (energy coupling rate) decreases rapidly with the separation distance. We expect that, in many areas of our sample, the distance between SLG and Si will be beyond vdW force interaction, resulting in a negligible local thermal conductance. The measured thermal conductance is an average over the whole probed region consisting of tight contact and loose contact regions. In other words, many ripples should exist in the SLG, leading to a rough contact with the Si substrate. Such loose contact will give graphene a lot of flexibility to thermally expand/contract without inducing strong strain/stress in graphene. This point is analyzed below in detail.

3.2. Weak Mechanical Coupling between SLG and Si. Our above measured very small interface thermal conductance indicates that the SLG has a loose contact with the Si substrate. This loose contact will have very limited constraint on graphene movement. This means that, under local heating, the thermal expansion mismatch at the interface will induce little stress in graphene. In other words, under local heating, the stress build-up in graphene can be used as an indicator to explore the local mechanical coupling strength. Weak mechanical coupling will lead to little stress in graphene and help explain the extremely weak interface energy coupling observed above.

To explore the SLG/Si interface mechanical coupling, the Raman wavenumber is evaluated under various heating levels. The wavenumber is related to both temperature and stress, and it is more sensitive to temperature than linewidth. The thermal expansion of SLG and Si should be considered in explaining the thermal stress in graphene if it arises. The thermal expansion coefficient of graphene was reported in a range from negative values to 1×10^{-5} K^{-1}.[27] At room temperature, the thermal

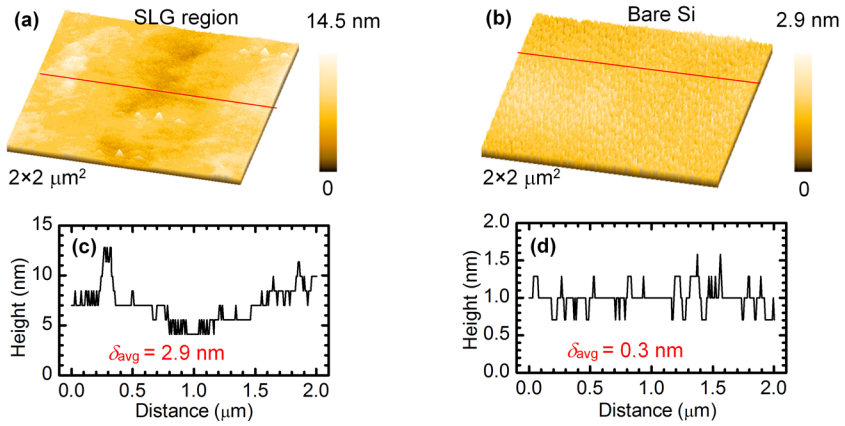

Figure 3. Nanoscale weak contact at the SLG/Si interface revealed by AFM. (a, b) AFM images of SLG/Si sample and bare Si. (c, d) The surface variations of the red lines shown in (a) and (b). For bare Si, the surface height varies around a certain location of 1.0 nm, and the variation observed in (d) mainly comes from the height measurement noise of ~0.3 nm. The surface is observed to be very flat. For SLG on Si shown in (c), the surface height varies with an amplitude as high as 9 nm. The average height of SLG above Si is 2.9 nm.

expansion coefficient of Si is about 2.6×10^{-6} K^{-1}.[28] There is a significant difference between thermal expansion coefficients of graphene and Si. During laser heating in our experiment, the degree of thermal expansion of graphene and Si is different. If tight bonding/mechanical coupling exists between them, then a large thermal stress would arise in graphene due to the thermal expansion mismatch. Otherwise, a loose contact would lead to a small/negligible stress.

3.2.1. Thermal Conductance Analysis Based on Raman Wavenumber. First of all, we evaluate the temperature rise in SLG and Si based on wavenumber while the stress effect is not subtracted and then use this temperature rise to calculate the interface thermal conductance. We intend to prove that, even under the effect of stress, the wavenumber method gives an interface thermal conductance very close to that determined on the basis of Raman linewidth analysis. This provides solid evidence that the stress in graphene and Si indeed is very small during the experiment and the mechanical coupling at the interface is weak. Then, we give quantitative analysis of the stress build-up in SLG and graphene.

The relationships between wavenumber temperature rise against heat flux for graphene and silicon are depicted in Figure 2c, along with their temperature coefficients of wavenumber from calibration. The slopes of wavenumber-based temperature rise against heat flux for SLG and Si are 6.74×10^{-3} Km^2W^{-1} (T'_{SLG}) and 8.40×10^{-4} Km^2W^{-1} (T'_{Si}), respectively. Using equation $G_t = 1/(T'_{SLG} - T'_{Si})$, the interfacial thermal conductance is calculated as 169 $Wm^{-2}K^{-1}$, with an uncertainty of 8.2 $Wm^{-2}K^{-1}$. This result is very close to the linewidth-method value of 183 $Wm^{-2}K^{-1}$. The similar thermal conductance results strongly conclude that the thermal stress in the sample is not significant. It needs to be pointed out that the calibration results shown in Figure 2c and the temperature determined using the wavenumber in Figure 2c all have the effect of stress build-up during calibration and laser-heating experiment. Below, we detail how to evaluate the stress build-up in graphene based on Raman wavenumber.

3.2.2. Stress Analysis for SLG and Si. In the laser heating experiment, at one specific laser heating level E, we could obtain the temperature of graphene, T_{SLG}, based on the Raman linewidth, which has little effect of stress. Using this temperature and the Raman wavenumber-T calibration result shown in Figure 2c, inset, an expected wavenumber shift for graphene can be calculated ($\Delta\omega_{cal}$). Note in calibration, SLG and Si have the same temperature, so $\Delta\omega_{cal}$ is the wavenumber shift of graphene at temperature T_{SLG} when the Si substrate is also at the same temperature. The interfacial thermal expansion mismatch between SLG and Si gives rise to a stress in graphene. Therefore, $\Delta\omega_{cal}$ consists of two parts: one by temperature rise, $\Delta\omega_{cal,T}$, and the other one by stress in graphene during calibration, $\Delta\omega_{cal,\sigma}$. In our interface thermal conductance measurement experiment, the temperature of SLG is always higher than that of Si substrate as shown in Figure 2a, and the graphene's wavenumber shift is directly measured as $\Delta\omega_{exp}$. Similarly, we also have $\Delta\omega_{exp} = \Delta\omega_{exp,T} + \Delta\omega_{exp,\sigma}$. Here, $\Delta\omega_{exp,T}$ should be equal to $\Delta\omega_{cal,T}$, but $\Delta\omega_{exp,\sigma}$ is the wavenumber shift induced by stress in graphene and should be different from $\Delta\omega_{cal,\sigma}$.

The above scenario can be better explained by Figure 2f. On the basis of the temperature rise shown in Figure 2a, we know that, when the temperature of SLG reaches 90 °C, the Si surface will have a temperature of 30 °C, but in calibration, when SLG is at 90 °C, the Si surface is at the same temperature. Thus, when the scenarios of calibration and laser heating experiment are compared, shown in Figure 2f, even the graphene has the same temperature, and the Si substrate has a contraction from calibration to the laser heating experiment. Therefore, this contraction will induce a stress change in graphene from calibration to the laser heating experiment. This Si contraction-induced wavenumber change in graphene can be calculated as $\Delta\omega_{exp} - \Delta\omega_{cal}$. The result is shown in Figure 2d. Similarly, we calculate the Raman wavenumber change by stress level change in Si and show the result in Figure 2d, too.

Figure 2d shows the stress induced wavenumber shift for SLG and Si. The compressive stress in SLG increases with the energy flux. The stress induced wavenumber shift is smaller than −0.09 cm^{-1}. This points out that the graphene placed on the Si substrate is loose and flexible. Graphene contracts/expands freely above the Si surface to a large degree during laser heating. The tight contact area between graphene and Si only counts a small part of the total graphene area. We feel confident that the separation between graphene and Si substrate is the main factor causing the poor thermal conductance/energy coupling at the interface. For Si, we observed negligible stress change in it between the calibration and the laser heating experiment. This again proves SLG and Si have a loose contact, and no tight mechanical coupling exists between them.

3.3. Weak Contact Revealed by Interface Raman Enhancement. *3.3.1. Surface Morphology Study.* The above interface energy coupling and strain/stress analysis of graphene leads to a conclusion that the SLG has a weak contact on the Si substrate. To further confirm this conclusion, we have conducted AFM imaging of the SLG on Si, and the results are shown in Figure 3a for SLG and Figure 3b for bare Si (for comparison purpose). The AFM images in Figure 3c,d show the height of surface variation for the SLG/Si and pure Si samples. For the AFM images of pure Si, the surface is found to be very flat within a height measurement noise of 0.3 nm. For SLG, the scenario becomes different. Ripples of SLG can be found in the image. The surface height varies with an amplitude as high as 9 nm, and the average height is 2.9 nm. Our above MD simulation gives an interfacial thermal conductance from 1.37×10^7 to 2.21×10^4 $Wm^{-2}K^{-1}$ when the separation distance increases from 0.4 to 0.7 nm. On the basis of the surface morphology revealed in Figure 3a, we conclude that only a very small portion of the graphene has sound contact and strong phonon coupling with the substrate, while large areas are separated from the Si surface.

3.3.2. Thermal Conductance Based on Raman Intensity with the Interference Effect. The rough contact and separation between SLG and Si will give rise to interference for the measured Raman signals. For this reason, Raman intensity is further processed to quantitatively explore the rough contact between SLG and Si. More importantly, with the help of light interference between SLG and Si, for the first time, we can evaluate the separation distance of these two layers using Raman intensity. It has been proved that Raman intensity drops with the increase of temperature. A higher temperature has more effect on the band structure, which imposes more restrictions on the photon interactions necessary to produce Raman scattering signals. Usage of absolute intensity difference is hard to determine the temperature rise, as intensity is sensitive to environmental factors, focal level of the probing laser, and configuration of the Raman system. To improve the measurement accuracy, normalized intensity is employed to determine temperature. The normalized Raman intensity variation of SLG and Si is calibrated at temperatures from 25 to 180 °C. Extrapolation is carried out to get the intensity value at 0 °C. The normalized intensity is the intensity normalized to that at 0 °C. The inset in Figure 2g shows that the normalized intensity decreases with temperature. The fitting slopes for G-band of SLG and Si are −0.00219 and −0.00235 K^{-1}, respectively. The coefficient of normalized intensity against temperature for Si is reported as −0.00249 K^{-1}.[29] To our best knowledge, no literature has reported the temperature coefficient for normalized intensity of graphene.

The slopes for temperature rise of SLG and Si against energy flux are 4.85×10^{-3} and 1.32×10^{-3} Km^2W^{-1}. The thermal conductance based on intensity is determined as 283 $Wm^{-2}K^{-1}$, as shown in Figure 2g, with an uncertainty of 16 $Wm^{-2}K^{-1}$. The temperature rise of Si obtained by intensity analysis is higher than that based on linewidth and wavenumber. As there is a separation between SLG and Si, part of the Si Raman signals is reflected by SLG. The collected Raman intensity of Si is reduced. Consequently, the temperature rise of Si determined by intensity reduction would increase. The thermal conductance obtained on the basis of the Raman intensity is larger than that based on linewidth and wavenumber. There are three factors combined together leading to this difference: deviated thermal expansion scenarios between experiment and calibration, the interface separation between SiC and Si, and light interference at the interface. Therefore, the difference between the temperature rise determined by Raman intensity and that by Raman linewidth strongly demonstrates the existence of separation between SLG and Si. Below, we detail the study of Raman enhancement by interface separation.

3.3.3. SLG/Si Interface-Induced Raman Enhancement. The thermal expansion of SLG and Si should be first considered in explaining the intensity effect. As mentioned above, there is a significant difference between thermal expansion coefficients of graphene and Si. In addition, the thermal expansion conditions in experiment and calibration are different, as illustrated in Figure 2f. We take a case of graphene at 90 °C for the analysis. In the calibration, the sample is heated up by a round heater which is glued under Si with silver paste. The temperatures of SLG and Si are the same and uniformly distributed within the Raman probing area (~8 μm^2). In calibration, the distance between SLG and Si is δ_{cal}, and the probed intensity is I_{cal}. In the laser heating experiment, the temperature distribution is different. Assume the temperature of SLG reaches the same level: 90 °C, the temperature of Si would be around 30 °C according to the linewidth method (Figure 2a). Therefore, Si shrinks relative to the scenario with temperature of 90 °C in calibration. Consequently, the height of the ripple of SLG on Si is enlarged, which means $\delta_{exp} > \delta_{cal}$, as illustrated in Figure 2f. This separation increase will lead to $I_{exp} > I_{cal}$, and the underlying physics is given below.

The Raman intensity enhancement factor (F) by interface gap increases with the thickness (δ) of the separation between SLG and Si if δ is not too large. In the experiment, the incident laser passes through the graphene flake since it only has one atomic layer. Raman scattering signal is generated because of the excitation of the incident laser. Both incident and Raman scattering lights are reflected multiple times on the air/SLG/air/Si interfaces. The interference effect on the Raman scattering signal enhances the Raman intensity. Considering the absorption and scattering of each layer, the normalized enhancement factor of Raman signal is calculated in 5.3 Interference Induced Raman Enhancement with optical constants of all layers according to previous work.[30,31] Figure 2h shows how the enhancement factor of Raman signal varies against the separation distance. The inset shows the enhancement factor with a very large separation variation.

According to the Raman intensity enhancement in the experiment, the thickness increment of air layer at the SLG/Si interface between the laser heating experiment and calibration can be evaluated. For instance, if under a laser heating energy flux E, the graphene has a temperature rise of ΔT. If the substrate has the same temperature as graphene just like in calibration, we expect the normalized Raman intensity (I_{cal}/I_0) from graphene will be $1 + \Delta T \cdot \chi_I$, where χ_I is the temperature coefficient of normalized intensity as shown in the inset of Figure 2g. Here, I_0 is the Raman intensity at room temperature, and I_{exp} is the expected Raman intensity. However, in our thermal conductance measurement experiment, the normalized Raman intensity of graphene with temperature rise ΔT is measured as I_{exp}/I_0. The enhancement of normalized Raman intensity can be calculated as $\Gamma_{nor} = (I_{exp}/I_0)/((I_{cal}/I_0) = (I_{mea}/I_0)/(1+\Delta T \cdot \chi_I))$. Due to the separation (δ) change as shown in Figure 2f, we expect Γ_{nor} will be greater than 1.

We take one laser heating case for quantitative analysis. From Figure 2a,g, when the absorbed energy flux in SLG is 1.0×10^4 Wm^{-2}, we have ΔT = 69.1 K, and χ_I = −0.00219/K. Our measured normalized Raman intensity at ΔT = 69.1 K is I_{exp}/I_0 =

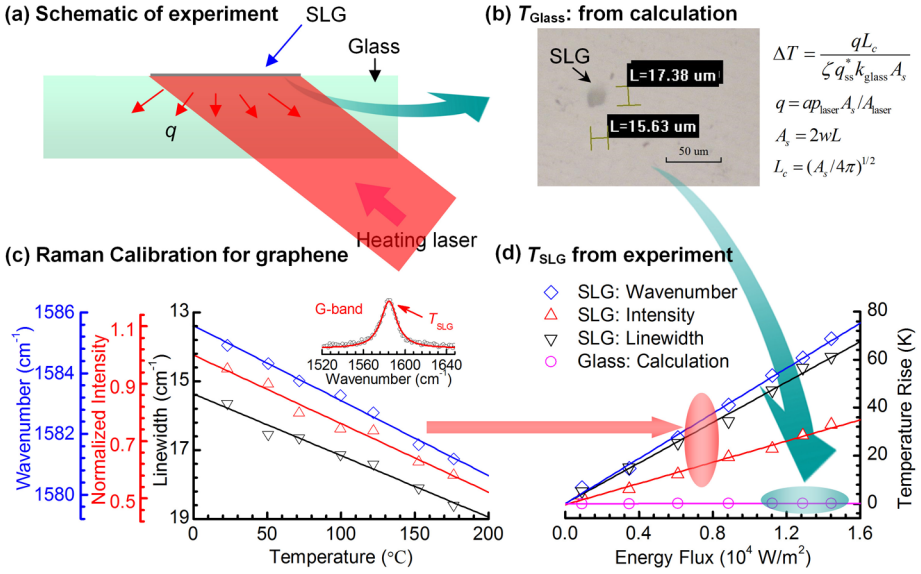

Figure 4. The SLG/glass interface energy coupling characterization. (a) Schematic of the experiment. (b) A heat transfer model is developed to calculate the temperature rise of the glass substrate that is heated up by SLG. The glass is treated as a semi-infinite plate. The area of SLG is delineated in the figure. (c) Calibration for temperature coefficient of SLG for wavenumber, normalized intensity, and linewidth. The fitting slopes for linewidth, wavenumber, and normalized intensity of SLG against temperature are 0.01791 cm^{-1}/K, -0.02471 cm^{-1}/K, and $-0.00239/K$, respectively. The Raman spectrum of G-band of SLG is shown in the inset. (d) The fitting slopes of experimental temperature rise of SLG against heating laser energy flux are 4.21×10^{-3}, 4.70×10^{-3}, and 2.21×10^{-3} Km^2W^{-1} based on the linewidth, wavenumber, and intensity methods, respectively. The slope of temperature rise of glass against heat flux is 4.54×10^{-4} Km^2W^{-1}. The interfacial thermal conductance is determined as 266 $Wm^{-2}K^{-1}$ according to the difference between the slope of the linewidth temperature of SLG and that of glass.

0.8866. The expected normalized Raman intensity without separation change is $(1 + \Delta T \cdot \chi_I) = 0.8488$. Therefore, we have $F_{nor} = 1.045$. On the basis of the AFM results, the original separation between SLG and Si is roughly $\delta_{cal} = 2.9$ nm. Therefore, the original enhancement would be $F_o = 1.019$ as shown in Figure 2h. After extra intensity enhancement by $\delta_{exp} \rightarrow \delta_{cal}$, the final enhancement factor is $F_h = F_o F_{nor} = 1.065$. F_o and F_h are illustrated in Figure 2h. Thus, on the basis of the enhancement calculation shown in Figure 2h, the final separation distance will be $\delta_{exp} = 4.7$ nm during laser heating with an energy flux of 1.0×10^4 Wm^{-2}. The separation increment of air layer is then obtained as $\Delta\delta = \delta_{exp} - \delta_{cal} = 1.8$ nm according to Figure 2h.

In the above calculation and discussion, the laser energy absorption in SLG is calculated following the optical path shown in Figure 1b. The interference effect is not considered since we do not know yet about the SLG/Si spacing then. Following the interference study above, we know that overall enhancement factor is 1.065. The absorption enhancement factor is less than this value; it is only 1.045. On the basis of this absorption enhancement factor, we can do a little adjustment of the thermal conductance calculated above. The thermal conductance calculated on the basis of the linewidth method is adjusted from 183 to 191 $Wm^{-2}K^{-1}$, and the one based on the wavenumber method is adjusted from 169 to 176 $Wm^{-2}K^{-1}$. Note this adjustment is only for the case of graphene temperature at 90 °C. For lower temperatures, the adjustment factor will be much less and eventually negligible.

From the above discussions, we conclude with great confidence that the contact between CVD graphene and Si substrate is poor. A separation layer exists at the interface, and this separation will increase under laser heating. The rough contact can be explained by the preparation method of the SLG/Si sample. In synthesis, a copper foil-based monolayer graphene was first prepared by the CVD method. Poly(methyl methacrylate) (PMMA) was then deposited on the graphene layer and cured. An etching process was taken to remove the copper foil. PMMA-SLG was washed in water and deposited onto Si substrate. After curing, PMMA was removed with acetone from the graphene layer. During this process, some residual atoms might stay between SLG and Si, which would reduce their contact significantly. Since the contact is loose, during laser heating, little stress arises and ripples become more obvious in the graphene layer.

3.4. Rough Contact between CVD Graphene and Glass.

Graphene has important applications in electronics and semiconductor devices when it is attached on a glass substrate. The contact condition and heat dissipation across the graphene/glass interface is critical to the stability and safety of devices. In this section, the rough contact and energy coupling at CVD graphene/glass interface is studied and compared with that at the CVD graphene/Si interface. The SLG/glass sample is obtained from ACS Material. The sample is prepared using the same process as that for SLG on Si.

The experimental setup for the thermal resistance measurement of SLG/glass interface is the same as that for the SLG/Si interface, except the heating laser irradiates the sample from the back of the glass substrate. At the wavelength ($\lambda = 1550$ nm) of the heating laser, little laser energy is absorbed in the glass. The graphene layer is heated up by the heating laser and dissipates heat crosses the interface to the glass substrate. A long integration time of 40 s is taken to collect strong Raman signals. The graphene layer is identified as monolayer according to the intensity ratio of 2D-band and G-band. The G-band of graphene is used for temperature probing of SLG layer. Since there is no Raman peak to characterize glass in our experiment, the temperature of glass cannot be determined precisely. Here, a heat conduction model is developed to calculate the surface temperature of glass.[32] Figure 4a,b shows the heat transfer model

dx.doi.org/10.1021/am405388a | ACS Appl. Mater. Interfaces 2014, 6, 2809−2818

and the area of the graphene layer. More details of the model are given in 5.4 Temperature Determination for SLG/Glass Interface. Under a laser power of 1.58 W, the glass surface increases by 0.15 K. The temperature rises of glass under different heat fluxes are calculated and shown in Figure 4d.

To determine the temperature rise of graphene, Raman linewidth, wavenumber, and intensity are all employed for comparison purposes. Calibration results for temperature coefficients of G-band of SLG are illustrated in Figure 4c. The temperature coefficients are 0.0179 cm^{-1}/K, −0.0247 cm^{-1}/K, and −0.00239/K for linewidth, wavenumber, and normalized intensity, respectively. Temperature rises of graphene under different laser heat fluxes are determined and shown in Figure 4d. The fitting slopes of temperature rise against heat flux are 4.21×10^{-3}, 4.70×10^{-3}, and 2.21×10^{-3} Km^2W^{-1} based on linewidth, wavenumber, and intensity, respectively. The calculated slope of temperature rise of glass against heat flux is 4.54×10^{-4} Km^2W^{-1}. Thus, the thermal conductance at the graphene/glass interface are determined to be 266, 235, and 568 $Wm^{-2}K^{-1}$, with uncertainties of 10.4, 6.8, and 36.5 $Wm^{-2}K^{-1}$, from the linewidth, wavenumber, and intensity methods, respectively. The small thermal conductance at the SLG/glass interface indicates a rough contact between them. We predict that only a very small portion of perfect contact between graphene and glass is in existence. A separation layer at major contact areas is expected to exist at the interface, which significantly slows the heat dissipation from graphene to glass. The thermal conductance calculated by wavenumber and linewidth agree well with each other. The difference in temperature obtained by wavenumber and linewidth stems from heat induced thermal stress in graphene, just as that detailed above for SLG on Si. The small difference illustrates that graphene experiences little stress. The bonding between graphene and glass is weak, and the graphene is loose. The thermal conductance based on the intensity method is about twice that based on linewidth, which further proves the rough contact at the interface as discussed for the SLG/Si interface. The thermal expansion coefficient of glass is about 5.5×10^{-7} K^{-1}, significantly different from that of graphene. The thermal expansion difference leads to mismatch under laser heating. Light interference happens due to the existence of the separation layer between graphene and glass. The interference effect on Raman signals at the SLG/air/glass interface enhances the Raman intensity. This intensity enhancement decreases the calculated temperature rise of graphene. Consequently, the thermal conductance based on intensity is larger than that based on linewidth and wavenumber. According to the foregoing discussions, the contact between CVD monolayer graphene and glass substrate is poor, probably at the same level as the SLG/Si interface.

Table 1 summarizes the experimental results on thermal conductance of graphene/substrate interfaces. The reported thermal conductance for graphene between sandwiched structures is between 2×10^7 and 2×10^8 $Wm^{-2}K^{-1}$ in the literature, which is much larger than our results. The changed flexural phonon behavior and contact condition at the interfaces lead to the improvement of interfacial heat transfer. The thermal conductance of interface between unconstrained graphene and substrate determined by Yue et al. is still larger than that in this work.[18] The reasons could be the difference in heating conditions and sample materials.

Table 1. Measured Thermal Conductance at Graphene/Substrate Interfaces

	materials	thermal conductance ($Wm^{-2}K^{-1}$)
our work	graphene/Si	183
our work	graphene/glass	266
Chen[14]	Au/SiO_2/graphene/SiO_2	$(0.8–1.8) \times 10^8$
Hopkins[15]	Al/graphene/SiO_2	2×10^7
Hopkins[15]	Al/O-graphene/SiO_2[a]	$(3–4) \times 10^7$
Koh[16]	Au/Ti/graphene/SiO_2	2.5×10^7
Mak[17]	graphene/SiO_2	$(0.5–1.1) \times 10^8$
Yue[18]	graphene/SiC	1.9×10^4

[a]O-graphene: oxygen functionalized sample.

4. CONCLUSION

We reported on energy coupling at the unconstrained graphene/substrate interface. Our novel localized photon excitation and thermal probing gave a thermal conductance at CVD graphene/Si and graphene/glass interfaces as 183 and 266 $Wm^{-2}K^{-1}$. These values are 5 orders of magnitude smaller than that for perfect interface contact. The observed extremely low interface energy coupling is attributed to nanoscale rough contact, which is confirmed by the flexible corrugation of graphene via analysis of stress-induced wavenumber change. Raman enhancement against heating further proved the existence of a gap between graphene and substrates. The structure study using AFM gave quantitative knowledge of graphene corrugation on a substrate.

5. METHODS AND EXPERIMENTS

5.1. Thermal Probing and Raman Calibration. The temperature coefficients of graphene and silicon Raman spectrum need to be calibrated first in order to determine the local temperature during the experiment. In the calibration, the same graphene/Si sample is placed on a heated stage, and the sample's temperature is controlled accurately. After the sample's temperature reaches steady state, Raman measurement is conducted to collect the Raman spectrum of both graphene and Si. The G peak (~1580 cm^{-1}) of graphene is employed for temperature determination. The Raman spectrum of graphene is fitted with the Lorentz function to determine precise Raman parameters. The Raman peak ~518 cm^{-1} of silicon is used for temperature determination of the Si substrate. The relationship between temperature and linewidth can be treated linearly within a small temperature range. The temperature coefficients of SLG and Si for linewidth are determined as 0.0255 and 0.00913 cm^{-1}/K, respectively, from room temperature to 180 °C, as shown in the inset of Figure 2a. Yue et al. obtained a temperature coefficient of trilayer graphene as 0.0127 cm^{-1}/K.[18] The temperature coefficient varies with the number of graphene layers. Tang et al. measured the temperature coefficient of Si and obtained a slope of 0.0082 cm^{-1}/K.[33] The work by Bauer et al. obtained a slope for temperature against linewidth as 0.01 cm^{-1}/K[34] for Si.

For wavenumber, it decreases with temperature with slopes of −0.0240 and −0.0201 cm^{-1}/K for G-band of SLG and Si, respectively. Yue et al. obtained a temperature coefficient of −0.025 cm^{-1}/K for triple layer graphene (TLG).[18] Others' work reported the slope of temperature against wavenumber in a range from −0.015 to −0.038 cm^{-1}/K for single and bilayer graphene.[35−37] The temperature coefficient varies with the number of graphene layers, the wavelength of the excitation laser, and the temperature range in the calibration. Calizo et al. pointed out that the temperature coefficient decreases with the number of layers.[36] The linear fitting slope of wavenumber against temperature for Si was reported as −0.022 cm^{-1}/K.[33,38] Therefore, the calibration results are in good agreement with the literature, considering the variation of experimental conditions and samples.

5.2. Result Interpretation Based on Atomistic Modeling of Interface Energy Coupling. Molecular dynamics simulation of thermal conductance at SLG/Si interface is carried out. A silicon layer

with dimensions of 5.8 × 20.0 × 5.4 nm^3 ($x \times y \times z$) is built and the supported graphene nanoribbon (GNR) is 4.1 × 18.3 nm^2 ($x \times y$). The second generation Brenner potential,[39] reactive empirical bond-order (REBO), based on the Tersoff potential[40,41] with interactions between C−C bonds is employed to model the graphene system. It has been proposed that the interactions between carbon atoms and the substrate are primarily the short-range vdW type.[42,43] Therefore, the C−Si coupling is modeled as vdW interaction using the Lennard-Jones (LJ) potential $V(r) = 4\varepsilon[(\sigma/r)^{12} - (\sigma/r)^6]$, where σ is the distance parameter, ε is the energy parameter, and r is the interatomic distance. In this work, ε and σ are set as 8.909 meV and 0.3326 nm, respectively.[44] The LJ potential is truncated at a cutoff distance of $r_c = 3.5\sigma$. The step for time integration is 0.5 fs (1 fs = 10^{-15} s). All MD simulations are performed using the large-scale atomic/molecular massively parallel simulator (LAMMPS) package.[26] Periodic boundary conditions are applied to the x and y directions (lateral direction), and free boundary condition is applied to the z direction for the physical domain shown in Figure 2b. The bottom layer of silicon substrate is fixed in position to avoid any vertical movement of the system. The two boundary layers of graphene in the y direction are fixed to maintain the distance between graphene and Si substrate. Four cases with separation distances (δ) of 0.4, 0.6, 0.65, and 0.7 nm are calculated, and the thermal conductance results are shown in Figure 2b.

Here, we take the 0.4 nm case as an example to show how the interface thermal conductance is determined. In modeling, after 300 ps canonical ensemble (NVT) and 100 ps microcanonical ensemble (NVE) calculations, the system reaches a thermal equilibrium at 300 K. Then, a thermal impulse with q_{in} of 6.04 × 10^{-4} W is added to the graphene system for 50 fs. After that, the graphene is left for thermal relaxation and its energy transfers to the substrate via the interface. The energy decay of graphene is governed by this equation: $E_t = E_0 + (G_tA)^{-1} \cdot \int_0^t (T_{GNR} - T_{Si})dt$. Here, A is the graphene area, E is graphene energy, and G_t is the interfacial thermal conductance. The subscripts "t" and "0" indicate graphene's energy at time t and the point immediately after the 50 fs pulsed heating. We track the energy relaxation of graphene for 150 ps and fit the $E_t \sim t$ curve using equation $E_t = E_0 + (G_tA)^{-1} \cdot \int_0^t (T_{GNR} - T_{Si})dt$ with different trial values of G_t. The trial value giving the best fit (least-squares) of the $E_t \sim t$ curve is taken as the interface thermal conductance. By fitting, the thermal conductance is calculated at 1.37 × 10^7 Wm^{-2}K^{-1} for the case with δ = 0.4 nm.

5.3. Interference Induced Raman Enhancement. The normalized enhancement factor of Raman signal is calculated with optical constants of all layers according to previous work.[30,31] The net absorption enhancement factor (F_{ab}) is expressed as

$$F_{ab} = t_1 \frac{(1 + r_2 r_3 e^{-2i\beta_2}) e^{-i\beta_x} + (r_2 + r_3 e^{-2i\beta_2}) e^{-i(2\beta_1 - \beta_x)}}{1 + r_2 r_3 e^{-2i\beta_2} + (r_2 + r_3 e^{-2i\beta_2}) r_1 e^{-2i\beta_1}} \quad (1)$$

where $t_1 = 2n_0/(n_0 + \tilde{n}_1)$, $r_1 = (n_0 - \tilde{n}_1)/(n_0 + \tilde{n}_1)$, $r_2 = (\tilde{n}_1 - \tilde{n}_2)/(\tilde{n}_1 + \tilde{n}_2)$, and $r_3 = (\tilde{n}_2 - \tilde{n}_3)/(\tilde{n}_2 + \tilde{n}_3)$ are the Fresnel transmittance and reflection coefficients for the interfaces involving air (0), SLG (1), air (2), and Si (3). n_0, $\tilde{n}_1$, $\tilde{n}_2$, and $\tilde{n}_3$ are the refractive indices for air, SLG, air, and Si, respectively. $\beta_x = 2\pi x\tilde{n}_1/\lambda$, $\beta_1 = 2\pi d_1\tilde{n}_1/\lambda$, and $\beta_2 = 2\pi d_2\tilde{n}_2/\lambda$, where x is the depth of the point where the interaction occurs, λ is the wavelength of incident laser, and d_1 and d_2 are the thickness of graphene layer and the in-between air layer, respectively.

The net scattering enhancement factor (F_{sc}) is described as

$$F_{sc} = t_1' \frac{(1 + r_2 r_3 e^{-2i\beta_2}) e^{-i\beta_x} + (r_2 + r_3 e^{-2i\beta_2}) e^{-i(2\beta_1 - \beta_x)}}{1 + r_2 r_3 e^{-2i\beta_2} + (r_2 + r_3 e^{-2i\beta_2}) r_1 e^{-2i\beta_1}} \quad (2)$$

where $t_1' = 2\tilde{n}_1/(\tilde{n}_1 + n_0)$ and λ is the wavelength of the G band of graphene. Thus, the total enhancement factor of Raman signal (F) is given by

$$F = N \int_0^{d_1} |F_{ab} F_{sc}|^2 dx \quad (3)$$

where N is a normalized factor, which is a reciprocal number of the total enhancement factor for a SLG layer on a Si substrate without the air layer between them, obtained by setting the thickness of the in-between air layer to be 0. In the calculation, the refractive index of graphene is 2.6 − 1.3i. The refractive indices of Si are 4.15 + 0.05i and 3.99 + 0.03i for incident laser and Raman scattering, respectively. Figure 2h shows how the enhancement factor varies against the separation distance.

5.4. Temperature Determination for SLG/Glass Interface. The experimental setup for the thermal measurement of SLG/glass interface is the same as that for the SLG/Si interface, except the irradiation direction of the heating laser. The heating laser reaches the glass layer from below with an angle of 60° to the vertical direction. The refractive indices for SLG and glass are 2.69 and 1.44, respectively. About 92.4% of the laser energy passes through the glass and reaches the SLG layer. The percentages of laser energy passing through the graphene are 83.6%, 26.8%, 2.9%, and 0.9% for the first four reflection processes of light, respectively. A total of 2.63% of incident laser energy is absorbed in SLG during the light propagation. Raman spectra of graphene were taken to determine the temperature rise of SLG, as shown in Figure 4c. A heat conduction model is developed to calculate the surface temperature of glass. Figure 4a,b shows the heat transfer model and the area of the graphene layer. In our experiment, heat transfers from a graphene flake to a semi-infinite glass plate. The heat transfer rate, q, can be expressed in the following equation:[32]

$$q = \zeta q_{ss}^* k_{glass} A_s \Delta T / L_c \quad (4)$$

where $q = a p_{laser} A_s / A_{laser}$, absorption a = 0.0263, laser power p_{laser} = (0.1−1.6) W, laser spot size $A_{laser} = 2.88 \times 10^{-6}$ m^2, ζ = 0.5 for a semi-infinite plate, graphene surface area $A_s = 2wL$, $w = 1.74 \times 10^{-5}$ m, $L = 1.56 \times 10^{-5}$ m, characteristic length $L_c = (A_s/4\pi)^{1/2}$, thermal conductivity of glass k_{glass} = 1.4 Wm^{-1}K^{-1}, dimensionless conduction heat transfer rate q_{ss}^* = 0.932, and ΔT is the temperature rise of glass surface. The temperature rises of glass under different heat fluxes are calculated and shown in Figure 4d.

AUTHOR INFORMATION

Corresponding Author

*E-mail: xwang3@iastate.edu. Tel: 515-294-8023. Fax: 515-294-3261.

Notes

The authors declare no competing financial interest.

ACKNOWLEDGMENTS

Support of this work by the National Science Foundation (CMMI-1200397 and CBET-1235852) is gratefully acknowledged.

REFERENCES

(1) Novoselov, K. S.; Geim, A. K.; Morozov, S. V.; Jiang, D.; Zhang, Y.; Dubonos, S. V.; Grigorieva, I. V.; Firsov, A. A. Electric Field Effect in Atomically Thin Carbon Films. *Science* **2004**, *306*, 666−669.

(2) Novoselov, K. S.; Geim, A. K.; Morozov, S. V.; Jiang, D.; Katsnelson, M. I.; Grigorieva, I. V.; Dubonos, S. V.; Firsov, A. A. Two-Dimensional Gas of Massless Dirac Fermions in Graphene. *Nature* **2005**, *438*, 197−200.

(3) Geim, A. K.; Novoselov, K. S. The Rise of Graphene. *Nat. Mater.* **2007**, *6*, 183−191.

(4) Zhang, Y. B.; Tan, Y. W.; Stormer, H. L.; Kim, P. Experimental Observation of the Quantum Hall Effect and Berry's Phase in Graphene. *Nature* **2005**, *438*, 201−204.

(5) Balandin, A. A.; Ghosh, S.; Bao, W.; Calizo, I.; Teweldebrhan, D.; Miao, F.; Lau, C. N. Superior Thermal Conductivity of Single-Layer Graphene. *Nano Lett.* **2008**, *8*, 902−907.

(6) Ghosh, S.; Calizo, I.; Teweldebrhan, D.; Pokatilov, E. P.; Nika, D. L.; Balandin, A. A.; Bao, W.; Miao, F.; Lau, C. N. Extremely High Thermal Conductivity of Graphene: Prospects for Thermal Management Applications in Nanoelectronic Circuits. *Appl. Phys. Lett.* **2008**, *92*, 151911.

(7) Lee, J.-U.; Yoon, D.; Kim, H.; Lee, S. W.; Cheong, H. Thermal Conductivity of Suspended Pristine Graphene Measured by Raman Spectroscopy. *Phys. Rev. B* **2011**, *83*, 081419.
(8) Ghosh, S.; Bao, W. Z.; Nika, D. L.; Subrina, S.; Pokatilov, E. P.; Lau, C. N.; Balandin, A. A. Dimensional Crossover of Thermal Transport in Few-Layer Graphene. *Nat. Mater.* **2010**, *9*, 555−558.
(9) Evans, W. J.; Hu, L.; Keblinski, P. Thermal Conductivity of Graphene Ribbons from Equilibrium Molecular Dynamics: Effect of Ribbon Width, Edge Roughness, and Hydrogen Termination. *Appl. Phys. Lett.* **2010**, *96*, 203112.
(10) Balandin, A. A. Thermal Properties of Graphene and Nanostructured Carbon Materials. *Nat. Mater.* **2011**, *10*, 569−581.
(11) Bolotin, K. I.; Sikes, K. J.; Hone, J.; Stormer, H. L.; Kim, P. Temperature-Dependent Transport in Suspended Graphene. *Phys. Rev. Lett.* **2008**, *101*, 096802.
(12) Du, X.; Skachko, I.; Barker, A.; Andrei, E. Y. Approaching Ballistic Transport in Suspended Graphene. *Nat. Nanotechnol.* **2008**, *3*, 491−495.
(13) Wu, Y. Q.; Ye, P. D.; Capano, M. A.; Xuan, Y.; Sui, Y.; Qi, M.; Cooper, J. A.; Shen, T.; Pandey, D.; Prakash, G.; Reifenberger, R. Top-Gated Graphene Field-Effect-Transistors Formed by Decomposition of SiC. *Appl. Phys. Lett.* **2008**, *92*, 092102.
(14) Chen, Z.; Jang, W.; Bao, W.; Lau, C. N.; Dames, C. Thermal Contact Resistance between Graphene and Silicon Dioxide. *Appl. Phys. Lett.* **2009**, *95*, 161910.
(15) Hopkins, P. E.; Baraket, M.; Barnat, E. V.; Beechem, T. E.; Kearney, S. P.; Duda, J. C.; Robinson, J. T.; Walton, S. G. Manipulating Thermal Conductance at Metal-Graphene Contacts via Chemical Functionalization. *Nano Lett.* **2012**, *12*, 590−595.
(16) Koh, Y. K.; Bae, M. H.; Cahill, D. G.; Pop, E. Heat Conduction across Monolayer and Few-Layer Graphenes. *Nano Lett.* **2010**, *10*, 4363−4368.
(17) Mak, K. F.; Lui, C. H.; Heinz, T. F. Measurement of the Thermal Conductance of the Graphene/SiO_2 Interface. *Appl. Phys. Lett.* **2010**, *97*, 221904.
(18) Yue, Y.; Zhang, J.; Wang, X. Micro/Nanoscale Spatial Resolution Temperature Probing for the Interfacial Thermal Characterization of Epitaxial Graphene on 4H-SiC. *Small* **2011**, *7*, 3324−3333.
(19) Wang, H.; Gong, J.; Pei, Y.; Xu, Z. Thermal Transfer in Graphene-Interfaced Materials: Contact Resistance and Interface Engineering. *ACS Appl. Mater. Interfaces* **2013**, *5*, 2599−2603.
(20) Xu, Z.; Buehler, M. J. Heat Dissipation at a Graphene−Substrate Interface. *J. Phys.: Condens. Matter* **2012**, *24*, 475305.
(21) Meyer, J. C.; Geim, A. K.; Katsnelson, M. I.; Novoselov, K. S.; Booth, T. J.; Roth, S. The Structure of Suspended Graphene Sheets. *Nature* **2007**, *446*, 60−63.
(22) Geringer, V.; Liebmann, M.; Echtermeyer, T.; Runte, S.; Schmidt, M.; Ruckamp, R.; Lemme, M. C.; Morgenstern, M. Intrinsic and Extrinsic Corrugation of Monolayer Graphene Deposited on SiO_2. *Phys. Rev. Lett.* **2009**, *102*, 076102.
(23) Nair, R. R.; Blake, P.; Grigorenko, A. N.; Novoselov, K. S.; Booth, T. J.; Stauber, T.; Peres, N. M. R.; Geim, A. K. Fine Structure Constant Defines Visual Transparency of Graphene. *Science* **2008**, *320*, 1308−1308.
(24) Graf, D.; Molitor, F.; Ensslin, K.; Stampfer, C.; Jungen, A.; Hierold, C.; Wirtz, L. Spatially Resolved Raman Spectroscopy of Single- and Few-layer Graphene. *Nano Lett.* **2007**, *7*, 238−242.
(25) Zhang, J.; Wang, Y.; Wang, X. Rough Contact Is Not Always Bad for Interfacial Energy Coupling. *Nanoscale* **2013**, *5*, 11598−11603.
(26) Plimpton, S. Fast Parallel Algorithms for Short-Range Molecular-Dynamics. *J. Comput. Phys.* **1995**, *117*, 1−19.
(27) Jiang, J. W.; Wang, J. S.; Li, B. W. Young's Modulus of Graphene: A Molecular Dynamics Study. *Phys. Rev. B* **2009**, *80*, 113405.
(28) Watanabe, H.; Yamada, N.; Okaji, M. Linear Thermal Expansion Coefficient of Silicon from 293 to 1000 K. *Int. J. Thermophys.* **2004**, *25*, 221−236.
(29) Tang, X.; Xu, S.; Wang, X. Nanoscale Probing of Thermal, Stress, and Optical Fields under Near-Field Laser Heating. *PLoS One* **2013**, *8*, No. e58030.
(30) Yoon, D.; Moon, H.; Son, Y. W.; Choi, J. S.; Park, B. H.; Cha, Y. H.; Kim, Y. D.; Cheong, H. Interference Effect on Raman Spectrum of Graphene on SiO_2/Si. *Phys. Rev. B* **2009**, *80*, 125422.
(31) Jung, N.; Crowther, A. C.; Kim, N.; Kim, P.; Brus, L. Raman Enhancement on Graphene: Adsorbed and Intercalated Molecular Species. *ACS Nano* **2010**, *4*, 7005−7013.
(32) Bergman, T. L.; Incropera, F. P.; Lavine, A. S.; DeWitt, D. P. *Fundamentals of Heat and Mass Transfer*, 7th ed.; John Wiley & Sons: New York, 2011.
(33) Tang, X.; Yue, Y.; Chen, X.; Wang, X. Sub-Wavelength Temperature Probing in Near-Field Laser Heating by Particles. *Opt. Express* **2012**, *20*, 14152−14167.
(34) Bauer, M.; Gigler, A. M.; Richter, C.; Stark, R. W. Visualizing Stress in Silicon Micro Cantilevers Using Scanning Confocal Raman Spectroscopy. *Microelectron. Eng.* **2008**, *85*, 1443−1446.
(35) Zhang, L.; Jia, Z.; Huang, L. M.; O'Brien, S.; Yu, Z. H. Low-Temperature Raman Spectroscopy of Individual Single-Wall Carbon Nanotubes and Single-Layer Graphene. *J. Phys. Chem. C* **2008**, *112*, 13893−13900.
(36) Calizo, I.; Balandin, A. A.; Bao, W.; Miao, F.; Lau, C. N. Temperature Dependence of the Raman Spectra of Graphene and Graphene Multilayers. *Nano Lett.* **2007**, *7*, 2645−2649.
(37) Allen, M. J.; Fowler, J. D.; Tung, V. C.; Yang, Y.; Weiller, B. H.; Kaner, R. B. Temperature Dependent Raman Spectroscopy of Chemically Derived Graphene. *Appl. Phys. Lett.* **2008**, *93*, 193119.
(38) Beechem, T.; Graham, S.; Kearney, S. P.; Phinney, L. M.; Serrano, J. R. Invited Article: Simultaneous Mapping of Temperature and Stress in Microdevices Using Micro-Raman Spectroscopy. *Rev. Sci. Instrum.* **2007**, *78*, 061301.
(39) Brenner, D. W.; Shenderova, O. A.; Harrison, J. A.; Stuart, S. J.; Ni, B.; Sinnott, S. B. A Second-Generation Reactive Empirical Bond Order (REBO) Potential Energy Expression for Hydrocarbons. *J. Phys.: Condens. Matter* **2002**, *14*, 783−802.
(40) Tersoff, J. Empirical Interatomic Potential for Carbon, with Applications to Amorphous-Carbon. *Phys. Rev. Lett.* **1988**, *61*, 2879−2882.
(41) Dodson, B. W. Development of a Many-Body Tersoff-Type Potential for Silicon. *Phys. Rev. B* **1987**, *35*, 2795−2798.
(42) Xiao, J. L.; Dunham, S.; Liu, P.; Zhang, Y. W.; Kocabas, C.; Moh, L.; Huang, Y. G.; Hwang, K. C.; Lu, C.; Huang, W.; Rogers, J. A. Alignment Controlled Growth of Single-Walled Carbon Nanotubes on Quartz Substrates. *Nano Lett.* **2009**, *9*, 4311−4319.
(43) Hertel, T.; Walkup, R. E.; Avouris, P. Deformation of Carbon Nanotubes by Surface van der Waals Forces. *Phys. Rev. B* **1998**, *58*, 13870−13873.
(44) Ong, Z. Y.; Pop, E. Molecular Dynamics Simulation of Thermal Boundary Conductance between Carbon Nanotubes and SiO_2. *Phys. Rev. B* **2010**, *81*, 155408.